Wind and Structures, *Vol. 23, No. 5 (2016) 385-403*
DOI: http://dx.doi.org/10.12989/was.2016.23.5.385

Across-wind dynamic loads on L-shaped tall buildings

Yi Li[1,3,4] and Qiu-Sheng Li[*2]

[1]School of Civil Engineering, Hunan University of Science and Technology, Xiangtan, 411201, Hunan, China
[2]Department of Architecture and Civil Engineering, City University of Hong Kong, Kowloon, Hong Kong
[3]College of Civil Engineering, Hunan University, Changsha, 410082, Hunan, China
[4]Hubei Key Laboratory of Roadway Bridge and Structure Engineering, Wuhan University of Technology, Wuhan, 430070, Hubei, China

(Received April 3, 2016, Revised July 14, 2016, Accepted July 22, 2016)

Abstract. The across-wind dynamic loads on L-shaped tall buildings with various geometric dimensions were investigated through a series of wind tunnel testing. The lift coefficients, power spectral densities and vertical correlation coefficients of the across-wind loads were analyzed and discussed in details. Taking the side ratio and terrain category as key variables, empirical formulas for estimating the across-wind dynamic loads on L-shaped tall buildings were proposed on the basis of the wind tunnel testing results. Comparisons between the predictions by the empirical formulas and the wind tunnel test results were made to verify the accuracy and applicability of the proposed formulas. Moreover, a simplified procedure to evaluate the across-wind dynamic loads on L-shaped tall buildings was derived from the proposed formulas. This study aims to provide a simple and reliable way for the estimation of across-wind dynamic loads on L-shaped tall buildings.

Keywords: tall buildings; wind tunnel testing; across-wind load; lift coefficient; power spectral density

1. Introduction

With the use of high strength materials and advanced constructional technology, modern tall buildings are becoming higher, lighter and more flexible than those in the past, resulting in the trend that the tall buildings are more sensitive to wind excitations. Davenport (1961, 1967) proposed a set of well-established methods to determine the wind loads and wind-induced responses of tall buildings in along-wind direction. However, accurate analytical calculation methods to evaluate across-wind dynamic responses of tall buildings are not available in the literatures. With the development of experimental technologies, extensive studies on the basis of wind tunnel tests indicated that the across-wind dynamic responses of tall buildings are generally larger than the along-wind responses (Saunders and Melbourne 1975, Kareem 1982, Solari 1985, Marukawa, Ohkuma *et al*. 1992, Choi and Kanda 1993, Kim, You *et al*. 2008, Gu, Cao *et al*. 2014, Isyumov, Ho *et al.* 2014). It has been recognized that the across-wind dynamic response is mainly caused by vortex shedding in the wake of a tall building. Due to the complex mechanisms of the wake excitation, it is very difficult to estimate the across-wind dynamic responses by analytical

∗Corresponding author, Professor, E-mail: bcqsli@cityu.edu.hk

http://www.techno-press.org/?journal=was&subpage=8 ISSN: 1226-6116 (Print), 1598-6225 (Online)

formulas. Based on the experimental results of the across-wind fluctuating forces obtained from wind tunnel tests, empirical formulas for the estimation of across-wind dynamic loads and responses were established and adopted in the design code of Japan (Tamura, Kawai *et al.* 1996). Liang, Liu *et al*. (2002) investigated the across-wind force spectra, RMS lift coefficients and Strouhal numbers of rectangular tall buildings based on results of a boundary layer wind tunnel testing and presented the mathematical model of across-wind dynamic loads on rectangular tall buildings. Gu and Quan (2004) obtained the first-mode generalized across-wind dynamic forces of 15 typical tall building models by use of high frequency force balance technique (HFBB), and proposed empirical formulas for power spectra of the across-wind dynamic forces, the coefficients of base moment and shear force. Ha (2013) conducted wind tunnel tests using aero-elastic models of rectangular prisms with various aspect and side ratios and formulated empirical equations for the across-wind fluctuating moment and spectral density. Xu and Xie (2015) established an empirical method to quickly assess the across-wind loads and accelerations of a tall building as a function of several parameters.

In recent years, more and more tall buildings with irregular and unconventional shapes have been built throughout the world. Lam, Wong *et al*. (2009) measured the dynamic wind loads on a number of H-shaped tall buildings with HFFB techniques and found that the fluctuations in the across-wind moments on H-shaped buildings were reduced comparing to those on rectangular shapes buildings. Kim and Kanda (2013) investigated the wind pressures on tapered and set-back tall buildings in wind tunnel testing, and pointed out that taper and set-back could affect the bandwidth of power spectra and position of peak frequencies of the across-wind forces. Mukherjee, Chakraborty *et al*. (2014) studied the pressure distributions on different faces of a 'Y' plan shaped tall building using both numerical and experimental means. Cheng, Lam *et al.* (2015) investigated the characteristics of fluctuating wind pressures on the side faces of H-shaped tall buildings and their role in the generation of across-wind forces with the space-time statistical tool of proper orthogonal decomposition.

Since the mechanisms of the wake excitation are strongly correlated with the shapes of tall buildings, it is necessary to investigate the across-wind dynamic loads and responses of tall buildings with irregular shapes. In this paper, eight L-shaped rigid tall building models with different geometric dimensions are tested by measurements of synchronous multi-pressure sensing system (SMPSS) in a boundary layer wind tunnel to study the characteristics of the across-wind dynamic loads on L-shaped tall buildings. Based on the experimental results, characteristics of the lift coefficients, power spectral densities and vertical correlation coefficients are discussed in details. Taking the side ratio of the tall building models and terrain type as two key elements, mathematic models of across-wind dynamic loads on L-shaped tall buildings are then proposed, which could be used for the wind-resistant design of L-shaped tall buildings.

2. Wind tunnel tests

Wind tunnel tests were conducted in a boundary layer wind tunnel at Hunan University, China. The working section of the wind tunnel is of 3.0 m wide, 2.5 m high and 20 m long, and the controllable wind speed ranges from 0 to 20 m/s. Spires and roughness elements were used to simulate the boundary layer wind flows specified in the Loads Standard Code of China (GB50009-2012, 2012). Four kinds of exposure conditions, including terrain categories A, B, C and D in accordance with the code, were simulated at a length scale of 1/500. The exponents of the mean wind speed profiles for terrain categories A, B, C and D are 0.12, 0.15, 0.22 and 0.30, and the corresponding gradient heights are 300 m, 350 m, 450 m and 550 m, respectively. The profiles of mean wind speed and longitudinal turbulence intensity simulated in the wind tunnel tests agreed well with those suggested in the code. The longitudinal velocity spectra for the terrain categories at the reference height of 0.6 m above the floor of the working section were in good agreement with the von Karman spectrum.

In order to investigate the characteristics of wind loads on L-shaped tall buildings, eight models with different L-shapes (called M1, M2, M3, M4, M5, M6 M7, M8) were made of ABS (Acrylonitrile Butadiene Styrene) material to ensure the strength and rigidity of the models., and a building model with rectangular section (called MR) was also adopted in this study for comparison purpose. M1, M2, M3, M5, M7, M8 are L-shaped models with different side ratios, while M4, M5, M6 are those with different aspect ratios. Table 1 lists the heights of each measurement layer on different models.

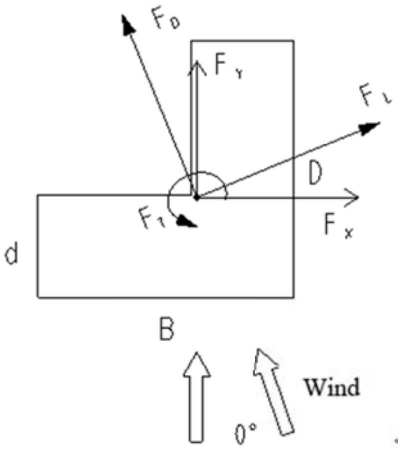

Fig. 1 Definition of wind loads

Fig. 2 L shaped building model in wind tunnel test

Table 1 Heights (mm) of each measurement layer on the models

Layer	M4	M1 ~ M3、M5、M7、M8	M6
1st	32	34	36
2nd	94	100	106
3rd	152	162	172
4th	206	220	234
5th	256	274	292
6th	302	324	346
7th	344	370	396
8th	382	412	442
9th	-	450	484
10th	-	484	522
11th	-	-	556
12th	-	-	586

Pressure measurements on the models were conducted for wind directions from 0° to 360° at an interval of 10°. Fig. 1 shows the definition of wind loads acting on the L-shaped building models. The mean wind speed at gradient height for all the wind tunnel tests was 12 m/s. Electronic pressure scanning modules made by Scanivalve Inc. (USA) were used to measure instantaneous pressures simultaneously. Data sampling frequency was set to be 312.5 Hz and the sampling length was 32s for each wind direction, which means that the total number of data obtained from a pressure tap was 10,000. A building model in the wind tunnel tests is shown in Fig. 2.

3. Results and discussions

Time series of across-wind dynamic loads at each measurement layer on an L-shaped model can be obtained by integrating the simultaneously measured fluctuating wind pressures. Mean and RMS lift coefficients are defined as

$$C_L(z_i) = \frac{\overline{F_L}(z_i)}{A(z_i)q_H} \qquad C_L^{'}(z_i) = \frac{\sigma_{F_L}(z_i)}{A(z_i)q_H} \tag{1}$$

$$C_{M_L} = \frac{\overline{M_L}}{BH^2 q_H} \qquad C_{M_L}^{'} = \frac{\sigma_{M_L}}{BH^2 q_H} \tag{2}$$

where, $C_L(z_i)$ and $C_L^{'}(z_i)$ are mean and RMS lift coefficients; $\overline{F_L}(z_i)$ and $\sigma_{F_L}(z_i)$ are mean and RMS across-wind forces at the height of z_i. C_{M_L} and C'_{M_L} are mean and RMS base moment coefficients in across-wind direction; $\overline{M_L}$ and σ_{M_L} are mean and RMS base moments. $A(z_i)$ is the frontal area of each measurement layer; B is the breadth in the direction perpendicular to the wind and H is the height of a model; $q_H = 0.5\rho U_H^2$ stands for the reference wind dynamic pressure, ρ is the air mass density, generally considered to be $1.25\, kg/m^3$, U_H is mean wind speed at the top of a model.

3.1 Lift coefficients

3.1.1 Effects of terrain category

Lift coefficients of the fourth layer of model M3 were chosen to investigate the effects of terrain category on the across-wind forces of L-shaped tall buildings. Fig. 3 shows the variation of the mean and RMS lift coefficients of model M3 for approaching winds over different terrain conditions with various wind directions. The terrain category almost has no influences on the mean lift coefficients under all wind directions, while it significantly affects the RMS lift coefficients. The RMS lift coefficients gradually increase as the turbulence intensity increases.

The variation of the mean lift coefficients is anti-symmetric about the wind direction of 225° while the variation of the RMS lift coefficients is symmetric about the wind direction of 225°. The mean lift coefficients range from -1.00 to 1.05 in all wind directions. The maximum and minimum values of the mean lift coefficients occur in the wind direction of 270° and 180°, respectively. The mean lift coefficients are nearly equal to zero when the incoming flow is around the wind directions of 45° and 225°. The RMS lift coefficients range from 0.10 to 0.50 in all wind directions. The maximum and minimum values of the RMS lift coefficients occur in the wind direction of 90° and 225°, respectively.

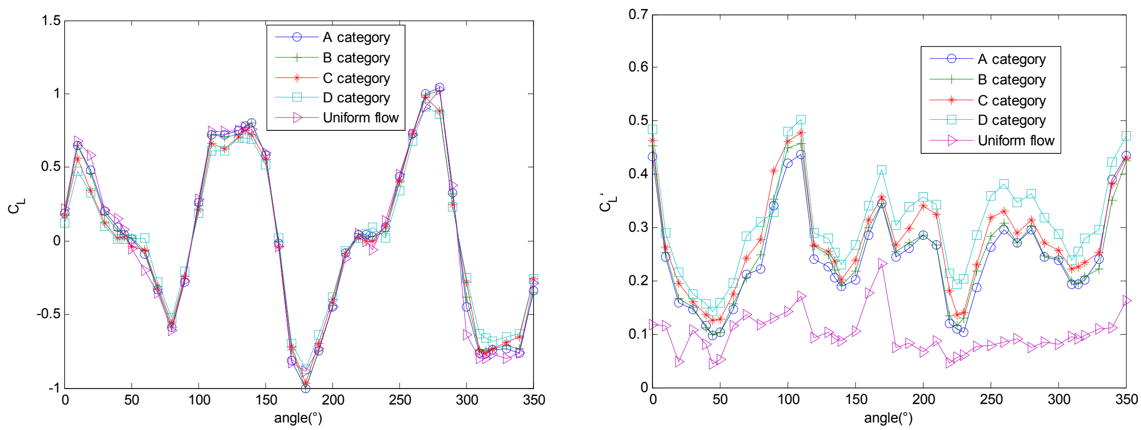

(a) Mean lift coefficients (b) RMS lift coefficients

Fig. 3 Variations of mean and RMS lift coefficients of model M3 for different terrain categories with wind direction

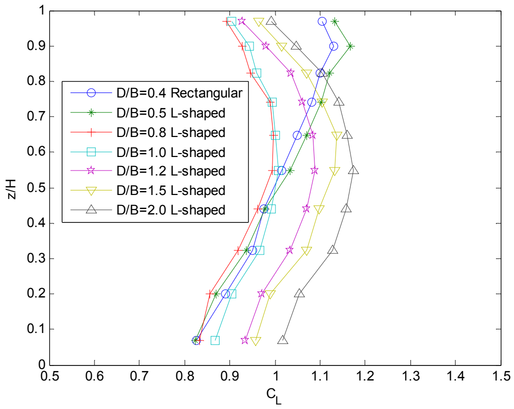

(a) Mean lift coefficients

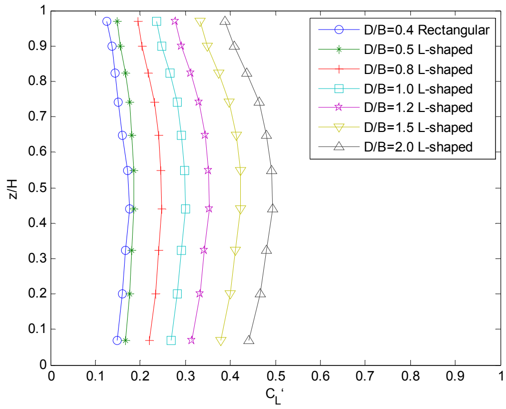

(b) RMS lift coefficients

Fig. 4 Variations of mean and RMS lift coefficients with the side ratio under the unfavorable wind direction

3.1.2 Effects of side ratio

The mean lift coefficients of rectangular tall buildings are close to zero when the incoming flow is perpendicular to the faces of a building. Therefore, only the RMS lift coefficients of rectangular tall buildings were discussed in previous studies (e.g., Lin, Letchford *et al.* 2005). However, for tall buildings with irregular shapes, the mean lift coefficients of L-shaped tall buildings are noteworthy. Since the unfavorable wind direction for the mean lift coefficients is different from that of the RMS lift coefficients, the wind directions of 270° and 90° were chosen to investigate the effects of the side ratio on the mean and RMS lift coefficients, respectively. Fig. 4 shows the variations of the mean and RMS lift coefficients under the unfavorable wind direction with different side ratios. As shown in Fig. 4, the mean lift coefficients of L-shaped models increase as the side ratio increases. When D/B≤0.5, the mean lift coefficients of L-shaped tall building models increase with the building height, except for those at the top layers of tall buildings due to the effects of three-dimensional flow. When D/B > 0.5, the mean lift coefficients of L-shaped models firstly increase and then decrease with the increase of the height, the maximum value is about 1.18 at approximately 0.55*H*. The RMS lift coefficients of L-shaped models also increase as the side ratio increases. When D/B≤0.5, the RMS lift coefficients at each layer are almost equal to 0.16. When D/B > 0.5, the RMS lift coefficients slightly increase from the bottom, and reach the peak at 0.55*H*, and then decrease as the height increases.

3.1.3 Effects of aspect ratio

Fig. 5 presents the variations of mean and RMS lift coefficients under the unfavorable wind direction with the aspect ratio of the building models. Both the mean and RMS lift coefficients increase as the aspect ratio increases, but the effects of the aspect ratio on the RMS lift coefficients are more significant. The mean lift coefficients reach the maximum value at the middle height of a model and then decrease rapidly as the height goes on to increase. The RMS lift coefficients decrease from the bottom of a model to 0.13 as the height increases.

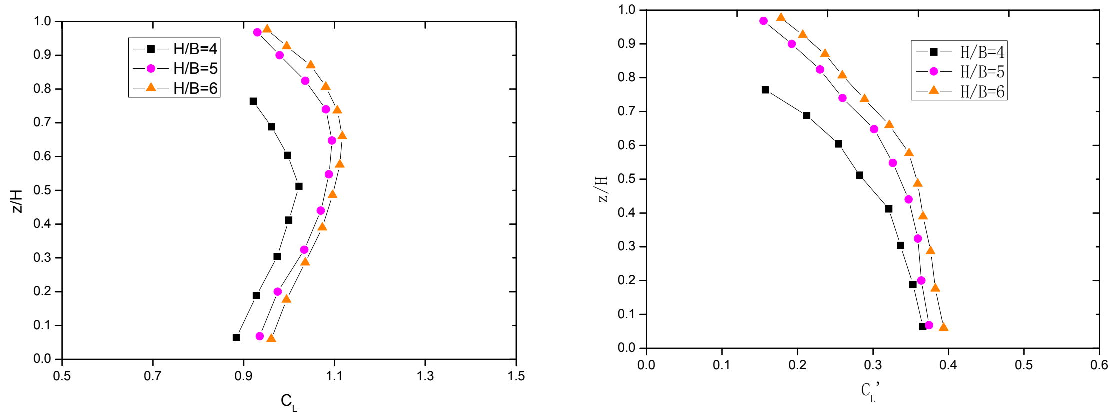

(a) Mean lift coefficients (b) RMS lift coefficients

Fig. 5 Variations of mean and RMS lift coefficients with the aspect ratio under the unfavorable wind direction

3.2 Base moment coefficients

The variations of the mean and RMS across-wind base moment coefficients with wind direction are shown in Fig. 6. The mean and RMS base moment coefficients vary with wind direction in consistent patterns with those of the lift coefficients. The mean base moment coefficients range from -0.85 to 0.75 in all wind directions and the RMS base moment coefficients range from 0.02 to 0.20. Both the mean base moment coefficients and the RMS base moment coefficients increase as the side ratio increases. The effects of the aspect ratio on the base moment coefficients in across-wind direction are relatively small.

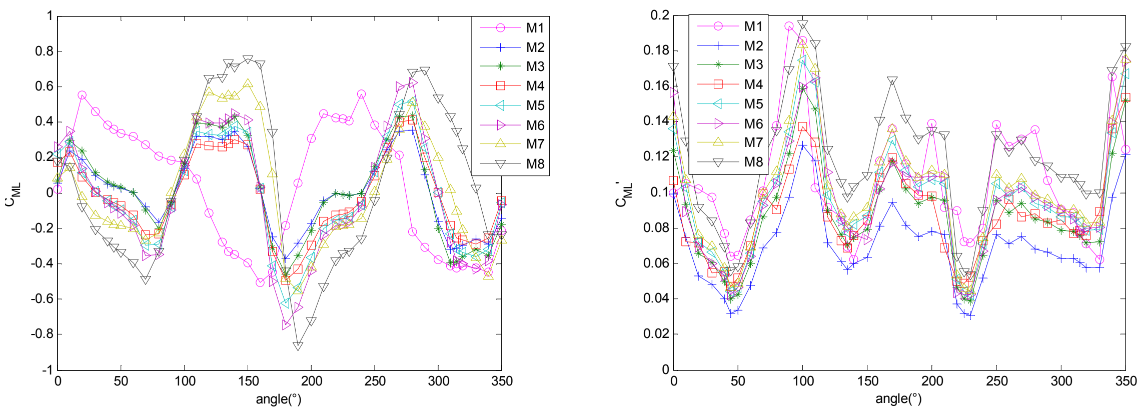

(a) Mean lift coefficients (b) RMS lift coefficients

Fig. 6 Variations of mean and RMS across-wind base moment coefficients with different wind directions

3.3 Power spectral densities

The power spectral densities of the across-wind dynamic loads were obtained for all the L-shaped models. Those at measurement layers B, D, F, H, K and basement of each model are presented herein to discuss the effects of elevation and the side ratio. Fig. 7 presents the across-wind force spectra of L-shaped models with various geometric dimensions over terrain category B. It can be found that the spectra of lift coefficients exhibit distinct narrow-bank peaks with different side ratios. As the side ratio increases, the energy of the peak magnitude gradually decreases and the reduced frequency corresponding to the peak point also decreases. Due to the shear-layer-edge interaction, the energy level of the across-wind force spectra is enhanced at the higher reduced frequency which is larger than the corresponding reduced frequency of the peak point, especially when the height of measurement layer is close to the top. In general, the across-wind basement force spectra are consistent with each other for different L-shaped models.

3.4 Mathematical model of across-wind dynamic loads on L-shaped tall buildings

The cross-spectral density of across-wind loads is essential to identify the dynamic wind loads acting on tall buildings. According to the knowledge of structural dynamics and theory of random vibration, the across-wind force spectrum for different heights can be determined by the following expressions

$$\begin{aligned} S_F(z_i,z_j;f) &= \sqrt{S_F(z_i;f)S_F(z_j;f)}Coh_F(z_i,z_j) = \\ &\sigma_F(z_i)\sigma_F(z_j)\sqrt{\frac{S_F(z_i;f)}{\sigma_F^2(z_i)}\frac{S_F(z_j;f)}{\sigma_F^2(z_j)}}Coh_F(z_i,z_j) \end{aligned} \tag{3}$$

where $S_F(z_i;f)$ and $S_F(z_j;f)$ are auto-spectra of wind loads at the heights of z_i and z_j, respectively ; $Coh_F(z_i,z_j)$ is coherence function of wind loads at the heights of z_i and z_j; $\sigma_F(z_i)$, $\sigma_F(z_j)$ are the RMS lift coefficients at the heights of z_i and z_j, respectively.

Based on the above analysis of power spectral density, non-dimensional spectrum of the basement is consistent with those of different measurement layers. Therefore, it can be regarded that

$$S_F^{'}(f) = \frac{S_F(z_i;f)}{\sigma_F^2(z_i)} = \frac{S_F(z_j;f)}{\sigma_F^2(z_j)} = \frac{S_{M_L}(f)}{\sigma_{M_L}^2} \tag{4}$$

where, $\frac{S_{M_L}(f)}{\sigma_{M_L}^2}$ stands for the non-dimensional spectrum of the basement.

Tang (2006) proved that the vertical coherence function $Coh_F(z_i,z_j)$ is equivalent to vertical correlation coefficient $Cor_F(z_i,z_j)$, and both are functions irrelevant with frequency. Therefore, Eq. (3) can be simplified as

$$S_F(z_i,z_j;f) = \sigma_F(z_i)\sigma_F(z_j)S_F^{'}(f)Cor_F(z_i,z_j) \tag{5}$$

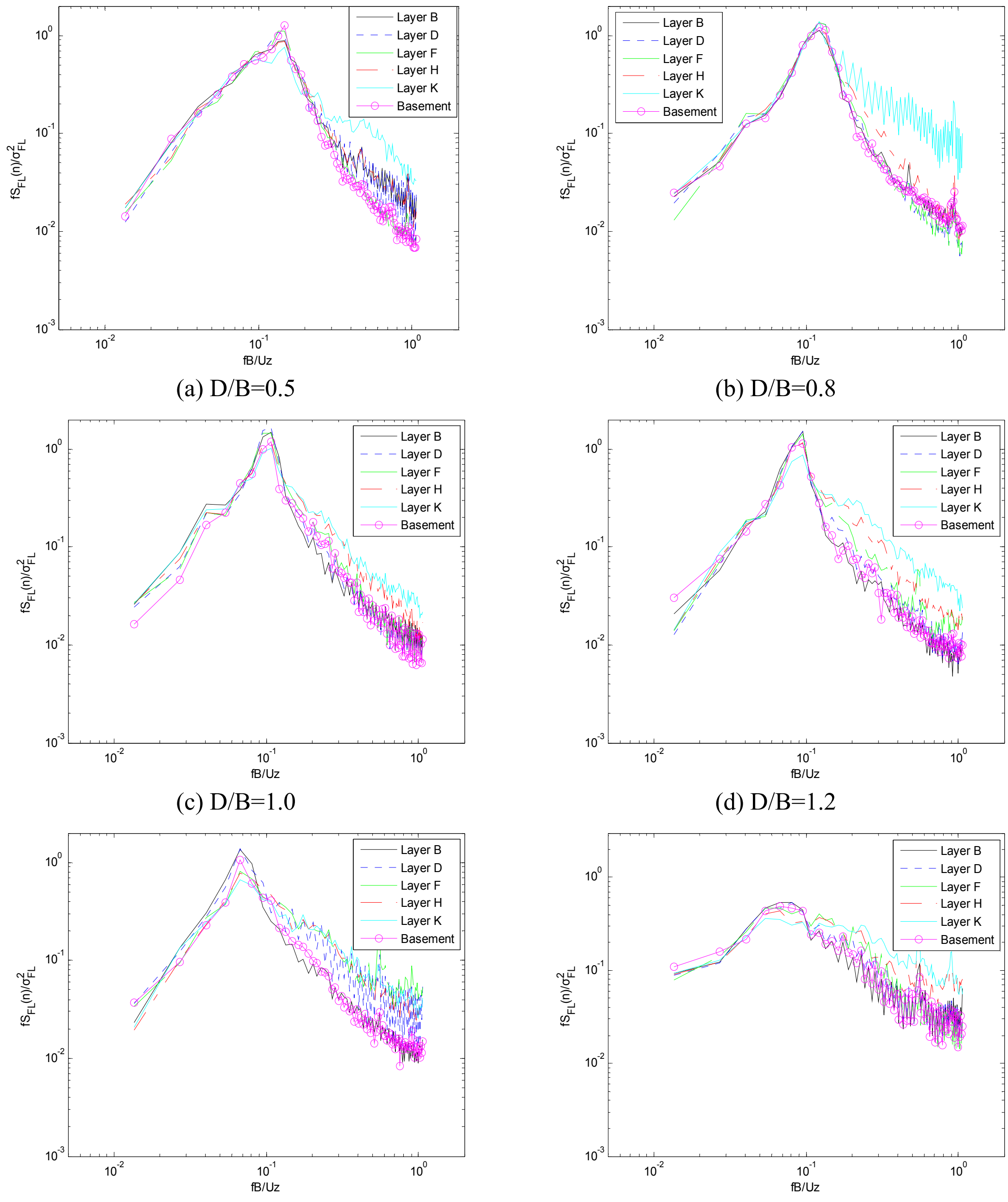

(a) D/B=0.5

(b) D/B=0.8

(c) D/B=1.0

(d) D/B=1.2

(e) D/B=1.5

(f) D/B=2.0

Fig. 7 Across-wind force spectra of L-shaped building models with various geometric dimensions

Non-dimensional spectra of the basement, RMS lift coefficients and vertical correlation coefficients are three key factors to calculate the cross-spectral density of the across-wind dynamic loads in Eq. (5). Since it is difficult or impossible to obtain the accurate value through theoretical analysis, numerical analysis based on wind tunnel test results is the common method to deal with this problem. The nonlinear least-squares method (NLSM) was adopted to establish empirical formulas based on the experimental results. The side ratio α_{DB} and terrain category α_{TR} are chosen as two key factors as follows

$$\alpha_{DB} = D / B \qquad \alpha_{DB} \in [0.5, 2.0] \tag{6}$$

$$\alpha_{TR} = \begin{cases} 1, & Category\ A \\ 2, & Category\ B \\ 3, & Category\ C \\ 4, & Category\ D \end{cases} \tag{7}$$

3.4.1 Power spectral density of base moment

The quasi-steady assumption is not suitable for the across-wind dynamic loading due to its complex mechanisms. Previous researches on the across-wind dynamic loads mainly focused on rectangular tall buildings, and empirical formulas of power spectral densities were established mainly based on wind tunnel testing results (Tamura, Kawai *et al*. 1996, Liang, Liu *et al*. 2002, Gu and Quan 2004). However, some limitations still existed in the existing formulas. For example, the formulas proposed by Tamura, Kawai *et al*. (1996) were only suitable for wind flows with lower levels of turbulence intensity (about 0.09). Liang, Liu *et al*. (2002) did not consider the effects of terrain categories. The formulas proposed by Gu and Quan (2004) were obtained by the HFFB technique in which the spatio-temporal characteristics of wind loads might not be considered due to the assumption of the linear mode. Moreover, all the existing power spectral densities are not available for L-shaped tall buildings. Hence, there is a need to establish such formulas. Based on the above discussions, the following normalized formula is proposed through the non-linear fitting of the wind tunnel testing results for the across-wind force spectra of L-shaped building models.

$$\frac{fS_{M_L}(f)}{\sigma_{M_L}^2} = \frac{S_p \beta (f_r / f_{sp})^\alpha}{\{1-(f_r / f_{sp})^2\}^2 + \beta (f_r / f_{sp})^2} + \frac{P \cdot (kf_r / f_{sp})^2}{(1+b(kf_r / f_{sp})^c)^d} \tag{8}$$

where, the first item $\dfrac{S_p \beta (f_r / f_{sp})^\alpha}{\{1-(f_r / f_{sp})^2\}^2 + \beta (f_r / f_{sp})^2}$ represents the contribution of vortex shedding; the second item $\dfrac{P \cdot (kf_r / f_{sp})^2}{(1+b(kf_r / f_{sp})^c)^d}$ stands for the contribution of turbulence from incoming flows.

Parameters S_p, f_{sp}, α, β, P, k, b, c and d in Eq.(8) are functions of the side ratio α_{DB} and the terrain category α_{TR}. These parameters were determined based on the wind tunnel testing results as follows

$$S_p = -1.6455\alpha_{TR}^2 + (7.3119\alpha_{TR} - 2.2151)\alpha_{DB} + (0.6448 - 4.3832\alpha_{TR})\alpha_{DB}^{2.5} + (1.8501 + 0.4009\alpha_{TR}^2)\alpha_{DB}^3 + (1.5570 + 0.3528\alpha_{TR}^2)\alpha_{DB}^{-1} \tag{9}$$

$$\beta = -0.0109 - 0.0292\alpha_{TR} + (0.0659 + 0.1582\alpha_{TR})\alpha_{DB} - (0.2917 + 0.2018\alpha_{TR})\alpha_{DB}^2 + (0.2918 + 0.1890\alpha_{TR})\alpha_{DB}^3 - (0.0665 + 0.1402\alpha_{TR})\alpha_{DB}^4 + (0.0117 + 0.0241\alpha_{TR})\alpha_{DB}^5 \tag{10}$$

$$f_{sp} = -1.1722 - 0.1104\alpha_{TR} + (0.4678 + 0.0819\alpha_{TR})\alpha_{DB} + (0.0080 - 0.0258\alpha_{TR})\alpha_{DB}^3 + (0.9587 + 0.1063\alpha_{TR})\alpha_{DB}^{-1} - (0.2273 + 0.0308\alpha_{TR})\alpha_{DB}^{-2} \tag{11}$$

$$\alpha = 5.2116 + 1.1046\alpha_{TR} - (1.1598 + 0.2571\alpha_{TR})\alpha_{DB} + (0.0133 + 0.0097\alpha_{TR})\alpha_{DB}^2 - (4.6304 + 1.2154\alpha_{TR})\alpha_{DB}^3 + (1.0131 + 0.6044\alpha_{TR})e^{\alpha_{DB}} \tag{12}$$

$$P = 0.2085 + 0.0670\alpha_{TR} + (0.9316 + 0.1952\alpha_{TR})\alpha_{DB}^2 - (1.1592 + 0.2628\alpha_{TR})\alpha_{DB}^4 + (0.5827 + 0.0978\alpha_{TR})\alpha_{DB}^6 - (0.0526 + 0.0317\alpha_{TR})\alpha_{DB}^8 \tag{13}$$

$$k = -92.2310 + 9.9038\alpha_{TR} + (49.7162 - 5.8371\alpha_{TR})\alpha_{DB} - (19.5719 - 2.8302\alpha_{TR})\alpha_{DB}^{1.5} - (67.0535 - 5.9709\alpha_{TR})\alpha_{DB}^{-0.5} - (9.2758 - 0.7662\alpha_{TR})\alpha_{DB}^{-1.5} \tag{14}$$

$$b = -122.4765\alpha_{TR}^{-2} - (0.9954 + 111.6770\alpha_{TR}^{-1})\alpha_{DB} - (0.0122 + 0.7609\alpha_{TR}^{-1})\alpha_{DB}^3 - (24.7728 + 85.7124\alpha_{TR}^{-2})\alpha_{DB}^{0.5}\ln(\alpha_{DB}) + (0.1692 + 0.6039\alpha_{TR}^{-2})\alpha_{DB}^{-2} \tag{15}$$

$$c = -5.3795 - 0.8391\alpha_{TR} - (0.7012 + 0.0967\alpha_{TR})\alpha_{DB} + (3.0556 + 0.6420\alpha_{TR}) \times \ln(\alpha_{DB}) + (6.4136 + 0.9235\alpha_{TR})\alpha_{DB}^{-0.5} - (0.1898 + 0.0271\alpha_{TR})\alpha_{DB}^{-2} \tag{16}$$

$$d = -0.0816 - 0.1591\alpha_{TR} + (0.8042 + 0.7996\alpha_{TR})\alpha_{DB}^{-1} - (1.9288 + 1.6508\alpha_{TR})\alpha_{DB}^{-2} + (1.7560 + 1.7420\alpha_{TR})\alpha_{DB}^{-3} - (0.9814 + 0.8009\alpha_{TR})\alpha_{DB}^{-4} + (0.1649 + 0.1504\alpha_{TR})\alpha_{DB}^{-5} \tag{17}$$

Taking terrain category B as an example, comparison of across-wind force spectra by the proposed formulas and the wind tunnel tests is shown in Fig. 8. It can be found from the figure that the spectra determined by the proposed formulas match well with those by the wind tunnel tests, indicating that the proposed formulas can provide reasonable predictions for the power spectra of the across-wind dynamic loads on L-shaped tall buildings. It should be pointed out that the force spectrum is very gentle when the side ratio is 2.0. This is similar to those of rectangular tall buildings (Liang, Liu *et al*. 2002) and related to the energy loss of vortex shedding caused by the increase of the side ratio.

The Strouhal number is widely used to describe the vortex shedding phenomenon of bluff body and only dependent on the shape of a building. With regard to the across-wind force spectra which are mainly contributed by vortex shedding, the Strouhal number is the reduced frequency corresponding to the peak point of such a spectrum. Compared the across-wind force spectra of the L-shaped models with various side ratio in Fig. 8, it is evident that as the side ratio increases, the reduced frequency corresponding to the spectral peak gradually decreases. By applying NLSM to fit the testing results, an empirical formula involved the side ratio as a variable for the Strouhal number of L-shaped buildings is established as shown in Eq. (18). Comparison of the Strouhal number by the proposed formula and the wind tunnel tests is shown in Fig. 9.

$$S_t = 0.2057 - 0.1232\alpha_{DB} + 0.0232\alpha_{DB}^2 \qquad 0.5 \le \alpha_{DB} \le 2 \tag{18}$$

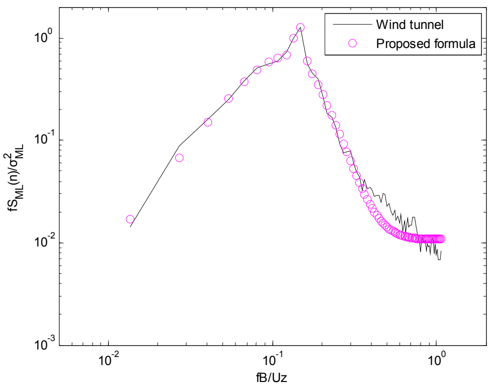

(a) D/B=0.5

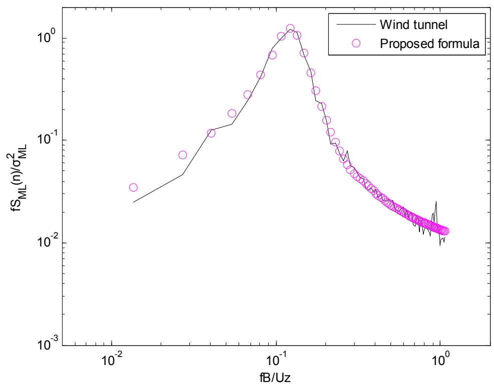

(b) D/B=0.8

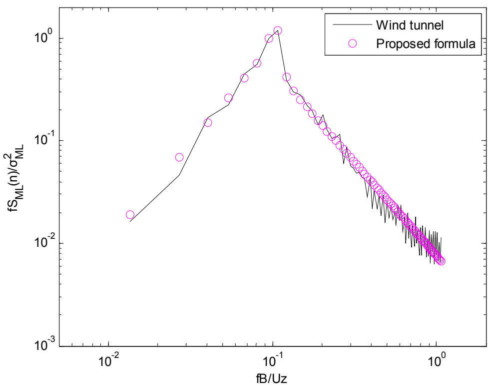

(c) D/B=1.0

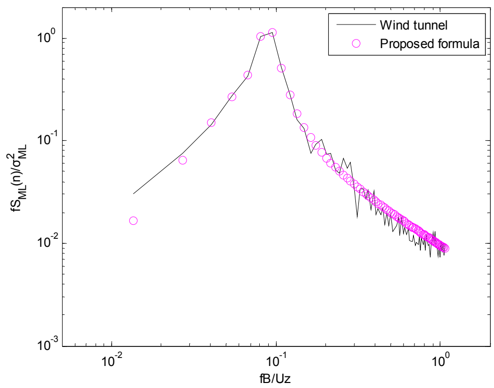

(d) D/B=1.2

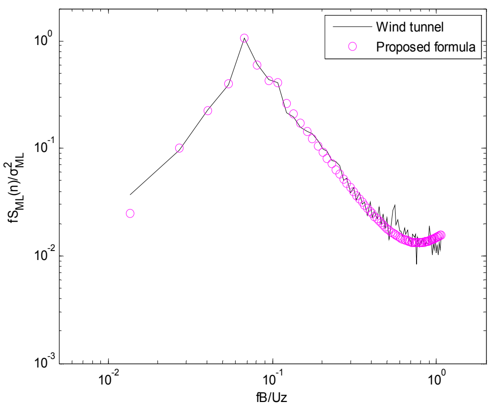

(e) D/B=1.5

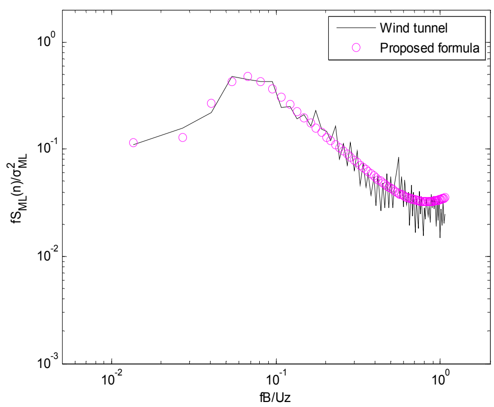

(f) D/B=2.0

Fig. 8 Comparisons of across-wind force spectra by the proposed formulas and the wind tunnel tests

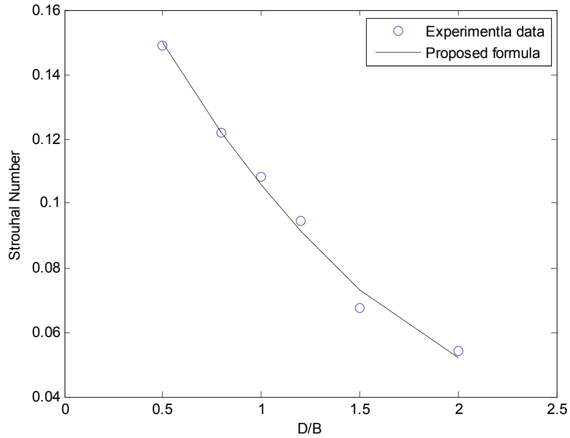

Fig. 9 Comparison of Strouhal number by the proposed formula and the wind tunnel tests

3.4.2 Lift coefficients

According to the discussion in **3.1**, the lift coefficients firstly increase and then decrease as the height of the measurement layer increases. Taking the relative height z/H as a parameter, the polynomial expression shown in Eq. (19) was used to fit the RMS lift coefficients of the L-shaped models, in which, $l_1^{'}, l_2^{'}, l_3^{'}$ and $l_4^{'}$ are model parameters. The NLSM was then adopted to fit the model parameters on the basis of the side ratio and the terrain category.

$$C_L^{'}(z) = l_1^{'} + l_2^{'}(\frac{z}{H}) + l_3^{'}(\frac{z}{H})^2 + l_4^{'}(\frac{z}{H})^3 \tag{19}$$

$$l_1^{'} = 0.0431 + 0.0130\alpha_{TR} + (0.1503 + 0.0135\alpha_{TR})\alpha_{DB} \tag{20}$$

$$\begin{aligned} l_2^{'} = & -0.0081 + 0.0238\alpha_{TR} + (0.2020 - 0.0600\alpha_{TR})\alpha_{DB} + (0.1236 - 0.0061\alpha_{TR})\alpha_{DB}^2 \\ & + (0.0014 - 0.0188\alpha_{TR})\alpha_{DB}^4 \end{aligned} \tag{21}$$

$$\begin{aligned} l_3^{'} = & \, 0.5265 - 0.2668\alpha_{TR} + (0.6403 - 0.3550\alpha_{TR})\alpha_{DB} - (0.2701 - 0.1296\alpha_{TR})\alpha_{DB}^3 \\ & + (0.2678 - 0.5498\alpha_{TR})e^{\alpha_{DB}} \end{aligned} \tag{22}$$

$$l_4^{'} = 0.0640 - 0.0214\alpha_{TR} + (0.0011 - 0.0722\alpha_{TR})\alpha_{DB} \tag{23}$$

Comparison of $C_L^{'}(z)$ between the results obtained from the wind tunnel tests and calculated by the empirical formulas is presented in Fig. 10. The maximum error is less than 4%, indicating the predictions based on the empirical formulas match with the test results well.

3.4.3 Vertical correlation coefficients

The correlation coefficients represent mutual dependence of two random variables. The vertical correlation coefficient $Cor_{F_L}(z_i, z_j)$ is defined as follows

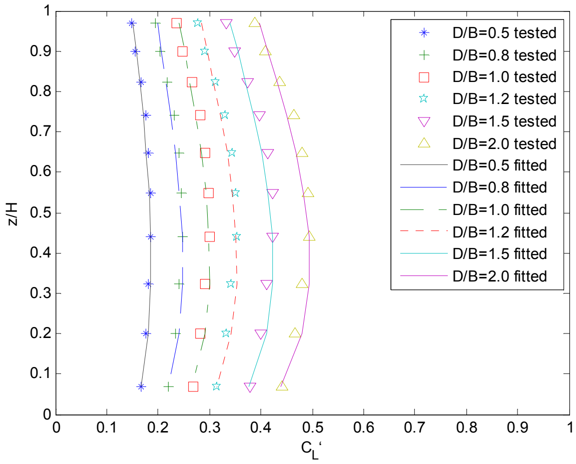

Fig. 10 Comparisons of lift coefficients by the proposed formula and the wind tunnel tests

$$Cor_{F_L}(z_i, z_j) = \frac{Cov_{F_L}(z_i, z_j)}{\sigma_{F_L}(z_i)\sigma_{F_L}(z_j)} \tag{24}$$

where, $Cov_{F_L}(z_i, z_j)$ is the covariance of lift coefficients between height z_i and z_j; $\sigma_{F_L}(z_i)$ and $\sigma_{F_L}(z_j)$ are the RMS lift coefficients at height z_i and z_j, respectively.

As shown in Fig. 11, when $D/B \le 1$, the vertical correlation coefficients of the neighboring measurement layers rapidly decrease as the relative height increases, but the results are scattered. When $D/B > 1$, the vertical correlation coefficients of the adjacent measurement layers near the base of the models gradually decrease as the side ratio increases and the vertical correlation coefficients of the adjacent layers at the upper half part remain around 0.3 ~ 0.5. Vickery and Clark (1972) indicated that the wake excitation made most contributions in across-wind dynamic responses and proposed a vertical correlation function for the wake excitation. However, the parameters in the correlation function are available only for some fixed side ratios. Based on the experimental results of this study, a new expression of vertical correlation coefficients is established as a function of the side ratio and the terrain category as follows

$$Cor_{F_L}(z_i, z_j) = \beta_L \times \exp(-\eta_L x) \tag{25}$$

where, $x = |z_i - z_j| / H$; β_L, η_L are parameters related with the side ratio and terrain category, and they can be determined as follows

$$\beta_L = 0.9005 + 0.0193\alpha_{TR} - (0.1435 + 0.0191\alpha_{TR})\alpha_{BD}^{-1} + (0.6175 + 0.0497\alpha_{TR})e^{-\alpha_{DB}} \tag{26}$$

$$\eta_L = 3.4145 - 0.1548\alpha_{TR} - (4.3205 - 0.2029\alpha_{TR})\alpha_{BD}^{-1} + (1.9300 - 0.0606\alpha_{TR})\alpha_{BD}^{-2} \tag{27}$$

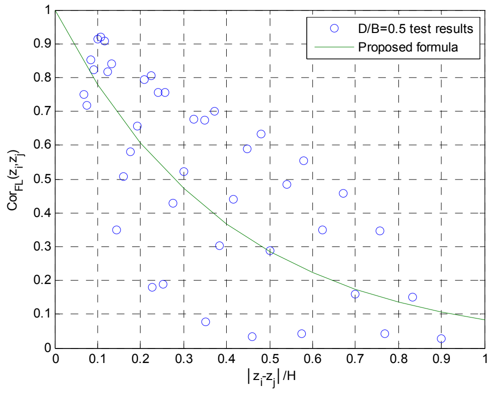

(a) D/B=0.5

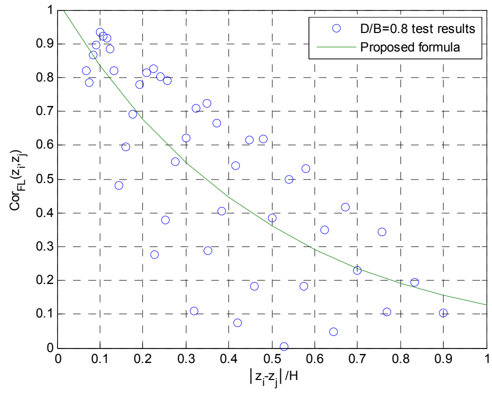

(b) D/B=0.8

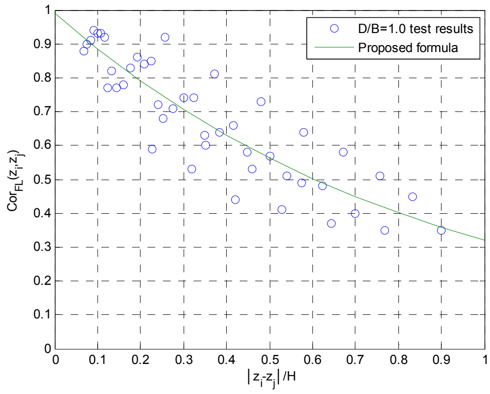

(c) D/B=1.0

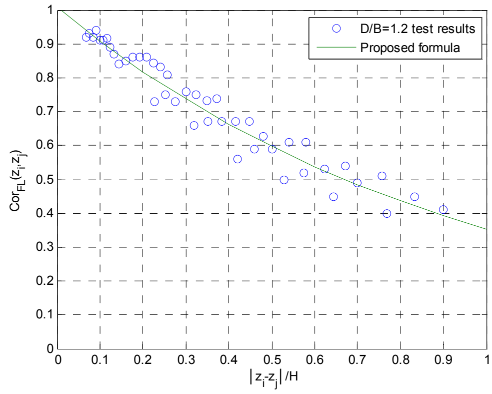

(d) D/B=1.2

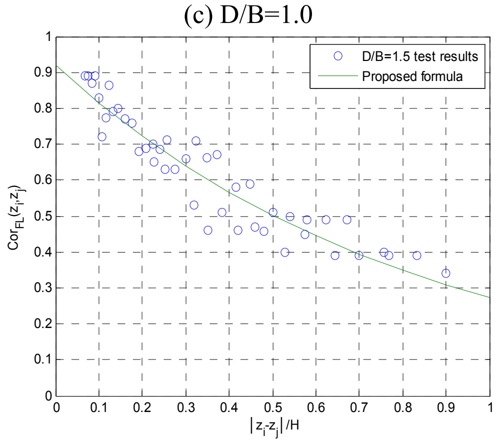

(e) D/B=1.5

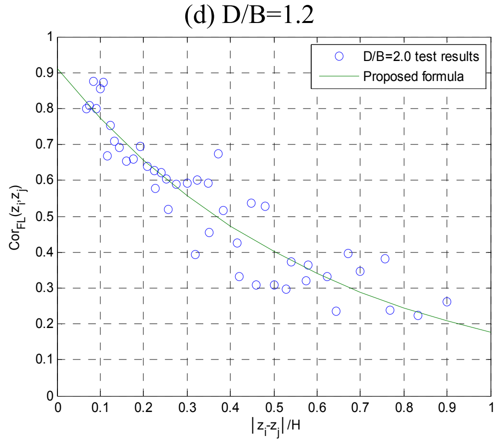

(f) D/B=2.0

Fig. 11 Comparisons of vertical correlation coefficients by the proposed formula and the wind tunnel tests

Curves in Fig. 11 show that the fitted results of the formula in terrain category B. When

$D/B>1$, the vertical correlation coefficients calculated by the formula are consistent with the experimental results. When $D/B\leq 1$, the curves basically represent that the vertical correlation coefficients vary with the relative height, although some discrepancies still exist between the predictions and the measurement results. In general, the proposed formula can effectively describe the characteristics of vertical correlation coefficients.

4. Conclusions

Based on the extensive wind tunnel tests, this paper investigated the characteristics of across-wind dynamic loads on L-shaped tall buildings. Lift coefficients, power spectral densities and vertical correlation coefficients were presented and discussed in details. The main conclusions from this study are summarized as follows:

(1) The changes of terrain category almost have no influences on the mean lift coefficients in all wind directions, but significantly affect the RMS lift coefficients. The RMS lift coefficients gradually increase as the level of turbulence intensity of approaching wind flows increases.

(2) The effects of the side ratio and the aspect ratio on the lift coefficients of L-shaped tall buildings were discussed under the unfavorable wind direction. In contrast with the aspect ratio, the side ratio has a more significant effect on the lift coefficients. Both the mean and RMS lift coefficients of L-shaped building models increase as the side ratio increases.

(3) The mean base moment coefficients range from -0.85 to 0.75 and the RMS base moment coefficients range from 0.02 to 0.20 in all wind directions. Both the mean base moment coefficients and the RMS base moment coefficients increase as the side ratio increases.

(4) The spectra of lift forces on L-shaped building models with different side ratios exhibit distinct narrow-band peaks. As the side ratio increases, the spectral peak magnitude gradually decreases and the reduced frequency corresponding to the peak point also decreases.

(5) When $D/B\leq 1$, the vertical correlation coefficients of adjacent measurement layers rapidly decrease as the relative height increases. When $D/B>1$, the vertical correlation coefficients of adjacent measurement layers near the base of the models gradually decrease as the side ratio increases and the vertical correlation coefficients of adjacent layers at the upper half part remain around $0.3\sim 0.5$.

(6) Taking the side ratio and the terrain category as two basic variables, empirical formulas of non-dimensional spectra of the basement, RMS lift coefficients and vertical correlation coefficients of L-shaped tall buildings were proposed in this study. Comparisons between the results by the proposed formulas and the wind tunnel tests were made to verify the accuracy of the proposed formulas. On basis of the formulas, a simplified procedure to estimate the across-wind dynamic loads is presented in the Appendix of this paper.

Acknowledgments

The work described in this paper was fully supported by a grant from National Nature Science Foundation of China (Project no: 51278439) and a grant from the Research Grants Council of Hong Kong Special Administrative Region, China (Project No: CityU 11256416). The authors would like to thank the support from Hubei Key Laboratory of Roadway Bridge and Structure Engineering in Wuhan University of Technology (Project no: DQJJ201502).

References

Cheng, L., Lam, K.M. and Wong, S.Y. (2015), "POD analysis of crosswind forces on a tall building with square and H-shaped cross sections", *Wind Struct.*, **21**(1), 63-84.

Choi, H and Kanda, J. (1993), "Proposed formula for the power spectral densities of fluctuating lift and torque on rectangular 3-D cylinders", *J. Wind Eng. Ind. Aerod.*, **42-47**, 507-516.

Davenport, A.G. (1961), "The application of statistical concepts to the wind loading of structure", *Proceedings of Institution of Civil Engineering.*, **19**, 449-472.

Davenport, A.G. (1967), "Gust loading factors", *J. Struct. Div. - ASCE*, **93**(3), 11-34.

GB50009-2012. (2012), Load Code for the Design of Building Structures. China Architecture & Building Press, Beijing.

Gu, M. and Quan, Y. (2004), "Across-wind loads of typical tall buildings", *J. Wind Eng. Ind. Aerod.*, **92**, 1147-1165.

Gu, M., Cao, H.L. and Quan, Y. (2014), "Experimental study of across-wind aerodynamic damping of super high-rise buildings with aerodynamically modified square cross-sections", *Struct. Des. Tall Spec. Build.*, **23**, 1225-1245.

Ha, Y.C. (2013), "Empirical formulations for evaluation of across-wind dynamic loads on rectangular tall buildings", *Wind Struct.*, **16**(6), 603-616.

Isyumov, N., Ho, E. and Case, P. (2014), "Influence of wind directionality on wind loads and responses", *J. Wind Eng. Ind. Aerod.*, **133**, 169-180.

Kareem, A. (1982), "Across wind response of buildings", *J. Struct. Div. - ASCE.*, **108**(4), 869-887.

Kim, Y.C. and Kanda, J. (2013), "Wind pressures on tapered and set-back tall buildings", *J. Fluid. Struct.*, **39**, 306-321.

Kim, Y.M., You, K.P. and Ko, N.H. (2008), "Across-wind responses of an aeroelastic tapered tall building", *J. Wind Eng. Ind. Aerod.*, **96**, 1307-1319.

Lam, K.M., Wong, S.Y. and To, A.P. (2009), "Dynamic wind loading of H-shaped tall buildings", *Proceedings of the Seventh Asia Pacific Conference*, Taipei, Taiwan.

Liang, S.G., Liu, S.C., Q.S. L., Zhang, L.L. and Gu, M. (2002), "Mathematic model of acrosswind dynamic loads on rectangular tall buildings", *J. Wind Eng. Ind. Aerod.*, **90**, 1757-1770.

Lin, N., Letchford, C., Tamura, Y., Liang, B. and Nakamura, O. (2005), "Characteristics of wind forces acting on tall buildings", *J. Wind Eng. Ind. Aerod.*, **93**(3), 217-242.

Marukawa, H., Ohkuma, T. and Momomura, Y. (1992), "Across wind and torsional acceleration of prismatic high rise buildings", *J. Wind Eng. Ind. Aerod.*, **42**(1-3), 1139-1150.

Mukherjee, S., Chakraborty, S., Dalui, S.K. and Ahuja, A.K. (2014), "Wind induced pressure on 'Y' plan shape tall building", *Wind Struct.*, **19**(5), 523-540.

Saunders, J.W. and Melbourne, W.H. (1975), "Tall rectangular building response to cross-wind excitation", *Proceedings of the 4th International Conference on Wind Effects on Buildings and Structures*, London, September.

Solari, G. (1985), "Mathematical model to predict 3-D loading on buildings", *J. Eng. Mech. - ASCE*, **111**(2), 254-275.

Tamura, Y., Kawai, Y., Uematsu, Y., Marukawa, H., Fujii, K. and Taniike, Y. (1996), "Wind load and wind-induced response estimations in the Recommendations for Loads on Buildings, AIJ 1993", *Eng. Struct.*, **18**(6), 399-411.

Tang, Y. (2006), "Research on the wind excited vibrations and static-equivalent wind loads of torsionally coupled high-rise buildings", Ph.D. Dissertation, Tongji University, Shanghai.

Vickery, B.J and Clark, A.W. (1972), "Lift or across-wind response of tapered stacks", *J. Struct. Div. - ASCE*,

1, 1-20.
Xu, Z.D. and Xie, J.M. (2015), “Assessment of across-wind responses for aerodynamic optimization of tall buildings”, *Wind Struct*., **21**(5), 505-521.

CC

Appendix: Estimation of across-wind dynamic loads on L-shaped tall buildings

According to the theory of random vibration, neglecting the effect of cross variance, the *kth* generalized force spectrum in across-wind direction can be expressed as

$$S_{F_k}^*(f) = \int_0^H \int_0^H S_{F_L}(z_i, z_j; f)\varphi_k(z_i)\varphi_k(z_j)dz_i dz_j \tag{28}$$

where, $\varphi_k(z_i)$, $\varphi_k(z_j)$ are the *kth* mode shape at the height of z_i and z_j .

When substituting Eq. (5) into Eq. (28) and combining Eq. (1), the *kth* generalized force spectrum can be simplified as follows

$$S_{F_k}^*(f) = \frac{(0.5\rho U_H^2)^2 A(z_i)A(z_j)S_{M_L}(f)}{\sigma_{M_L}^2} \times \int_0^H \int_0^H C_L^{'}(z_i)C_L^{'}(z_j)Cor_{F_L}(z_i, z_j)\varphi_k(z_i)\varphi_k(z_j)dz_i dz_j \tag{29}$$

where the expressions for $\dfrac{S_{M_L}(f)}{\sigma^2{}_{M_L}}$, $C_L^{'}(z)$ and $Cor_{F_T}(z_i, z_j)$ have been given in this paper.

The spectrum of the displacement response of the *kth* mode is

$$S_{Y_k}^*(f) = \frac{S_{F_k}^*(f)}{M_k^2}\left|H_k(f)\right|^2 \tag{30}$$

in which, $M_k = \int_0^H m(z_i)\varphi_k(z_i)dz_i$ is the *kth* generalized mass of the concerned building.

$\left|H_k(f)\right|^2 = \dfrac{1}{(2\pi n_j)^4\left\{\left[1-(n/n_j)^2\right]^2 + (2\varsigma_j n/n_j)^2\right\}}$ is the frequency response function of the *kth* mode.

The dynamic displacement response is regarded to be zero mean stationary random process. Therefore, the *kth* RMS displacement response can be determined by

$$\sigma_{Y_k} = \sqrt{\int_0^\infty S_{Y_k}^*(f)df} \tag{31}$$

The relationship between the acceleration response spectrum and the displacement response spectrum is

$$\mathrm{S}_{\ddot{\mathrm{Y}}_k}^*(\mathrm{f}) = \left(2\pi \mathrm{f}\right)^4 \mathrm{S}_{\mathrm{Y}_k}^*(\mathrm{f}) \tag{32}$$

Then, the RMS across-wind acceleration of the *kth* mode can be calculated by

$$\sigma_{\ddot{Y}_k} = \sqrt{\int_0^\infty (2\pi f)^4 S_{Y_k}^*(f)df} \tag{33}$$